Enhanced Dual-Stage Correlated Diffusion Imaging

Farzad Khalvati, Junjie Zhang, Masoom A. Haider, Alexander Wong

***Abstract*— Prostate cancer is the most common form of cancer and third leading cause of cancer death in Canadian men. Multi-parametric magnetic resonance imaging (mpMRI) has become a powerful non-invasive diagnostic tool for the detection of prostate cancer. Among mpMRI imaging modalities, diffusion-weighed imaging has shown the most promising results in accurate detection of prostate cancer. Introduced recently, correlated diffusion imaging (CDI) is a new form of diffusion imaging which accounts for the joint correlation of diffusion signal attenuation across multiple gradient pulse strengths and timings to improve the separability of cancerous and healthy tissues. Dual-stage CDI (D-CDI) is a newer generation of CDI where in contrast to CDI that does not capture anatomical information, an additional signal mixing stage between the correlated diffusion signal from the first signal mixing stage (CDI) and an auxiliary diffusion signal is performed to incorporate anatomical context. The core of D-CDI is a signal mixing algorithm that combines diffusion images at different b values to construct a single image. In this paper, we enhance the signal mixing algorithm to optimize the contribution of each single b-value image to maximize the separability of cancerous and healthy tissues. We evaluated the enhanced D-CDI (eD-CDI) using area under the ROC curve for datasets of 17 patient cases with confirmed prostate cancer and the results show that eD-CDI outperforms the original D-CDI as well as T2 weighted images and diffusion-weighed images used in the form of apparent diffusion coefficient maps.**

I. INTRODUCTION

Prostate cancer is the most common form of cancer and third leading cause of cancer death diagnosed in Canadian men, with more than 23,500 new cases and 4,100 deaths in 2015 [1]. Nevertheless, if diagnosed early, the survival rate of prostate cancer is relatively high [2]. Therefore, it is crucial to have a reliable and accurate screening method in place to detect and diagnose clinically significant prostate cancers early enough to allow for the right course of treatment to be taken if necessary.

Prostate Specific Antigen (PSA) screening has been shown to result in overtreatment and overdiagnosis of prostate cancer reducing the quality of life [3], [4]. Furthermore, biopsy-based Gleason score suffers from sampling issues where in some cases the index tumour is entirely missed. It has also become increasingly clear that prostate biopsies are harmful resulting in increased hospital admission rates due to infectious complications [5]. Recent advances in multi-parametric magnetic resonance imaging (mpMRI) of prostate have shown promise in improving the accuracy of diagnosis with mpMRI being more closely correlated with the prostatectomy Gleason score than the pre-operative biopsy. By capturing the entirety of cancer site and the ability to reconstruct 3D images, mpMRI has the distinct advantage of assessment of tissue heterogeneity, a well described phenomenon in cancer analysis with varying cell phenotypes. Nevertheless, mpMRI readings suffer from interobserver variability and some clinically significant cancers are still missed [6].

To overcome the shortcomings of conventional qualitative assessments of mpMRI, as part of a clinical decision support system, automated prostate cancer algorithms that generate and utilize the quantitative imaging features have been the focus of several research groups in recent years. These computer-aided detection (CAD) tools aim for helping radiologists in interpreting images more accurately and more consistently [7], [8], [9]. Specifically, mpMRI which combines T2-weighted MRI (T2w), diffusion-weighted imaging (DWI), and dynamic contrast enhanced imaging (DCE) has been extensively used for prostate cancer diagnosis by different prostate cancer CAD algorithms. By taking advantage of the unique information provided by each individual imaging technique, mpMRI can provide the CAD algorithms with the different characteristics of prostate tissue to improve the separability between cancerous and healthy tissues. Although DCE is considered as part of mpMRI, because it requires invasive contrast agent, T2w and apparent diffusion coefficient (ADC) map together are considered as the most commonly used mpMRI modality.

Computational diffusion-weighted MRI (CD-MRI) are DWI sequences that have been generated computationally with the goal of harnessing the information embedded in mpMRI but not captured by conventional sequences of DWI. Particulary, computed high b-value (b-values greater than $1,000 s/mm^2$) DWI (CHB-DWI) has been proposed as an alternative approach to actual high b-value DWI, which cannot be obtained due to hardware limitations, where a computational model is used to reconstruct DWI imagery at high b-values using low b-value DWI acquisitions [10], [11].

CD-MRI has also been used in designing CAD tools where CHB-DWI has been extensively used to improve the performance of CAD algorithms for prostate cancer [7]. While CHB-DWI reconstructs an image at a high b-value using low b-value images, correlated diffusion imaging (CDI) was proposed to combine the existing b-value images in a way so that the tissue being imaged is characterized by

This work was partially supported by the Natural Sciences and Engineering Research Council of Canada (NSERC), Ontario Institute of Cancer Research (OICR), and Cancer Care Ontario (CCO)-Imaging Network of Ontario (CINO).

Farzad Khalvati, Junjie Zhang, and Masoom A. Haider are with the Department of Medical Imaging, University of Toronto and Sunnybrook Research Institute, Toronto, Ontario, Canada, M4N 3M5. farzad.khalvati@sri.utoronto.ca

Alexander Wong is with the Department of Systems Design Engineering, University of Waterloo, Waterloo, Ontario, Canada, N2L 3G1.

the joint correlation of diffusion signal attenuation across multiple gradient pulse strengths and timings [12]. By taking advantage of information available across multiple gradient pulse strengths and timings, CDI improves the separability of cancerous and healthy tissue while reducing the need for gradient pulse fine-tuning [12].

While CDI was shown to improve the signal delineation between cancerous tissue and healthy tissue within the prostate gland [7], [13], one limitation it faced was the lack of anatomical information where it more or less looked as a binary image making it challenging for a radiologist to perform a visual assessment and accurate cancer localization. To overcome this limitation, dual-stage CDI (D-CDI) was proposed in which an additional signal mixing stage was performed between the correlated diffusion signal from the first signal mixing stage (CDI) and an auxiliary diffusion signal or T2w image to incorporate anatomical context [14] (Figure 1).

In this paper, we present enhanced D-CDI, *eD-CDI*, in which a new formulation is introduced that extends greatly upon the signal mixing formulation in D-CDI to allow for an optimal cancerous-healthy tissue delineation. In eD-CDI, the contribution of each individual b-value image to the signal mixing is optimized in order to maximize the performance of the final correlated diffusion signal (i.e., eD-CDI) with respect to the delineation of cancerous and healthy tissues within the prostate gland. As it will be shown in the upcoming sections, eD-CDI outperforms the original D-CDI as well as the conventional mpMRI namely T2w and ADC modalitites.

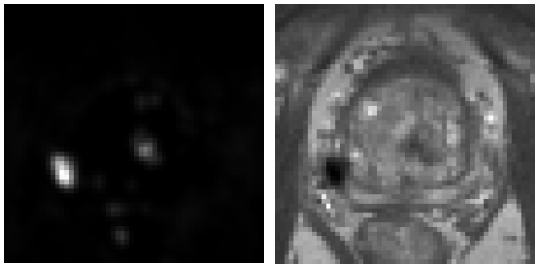

(a) CDI (b) D-CDI

Fig. 1: A sample prostate image shown in CDI and D-CDI modalitites [14].

II. METHODOLOGY

The methodology of the dual-stage CDI (D-CDI) is summarized in Fig. 2. First, several diffusion signals are acquired at different gradient pulse strengths and timings. Next, the acquired diffusion signals are mixed computationally to obtain the local correlation of signal attenuation across the acquired signals. Finally, in order to include anatomical context, an auxiliary diffusion signal (e.g., b_0 image) or T2w image is mixed with the correlated diffusion signal of the first signal mixing stage oC_1. In enhanced D-CDI or *eD-CDI*, the signal mixing stages also contain an optimization stage where the contribution of each diffusion signal is controlled to maximize the delineation of cancerous and healthy tissues in the final image oC_2. This is done by using some coefficients (α_i, τ_b, τ_{C_1}) as inputs to signal mixers.

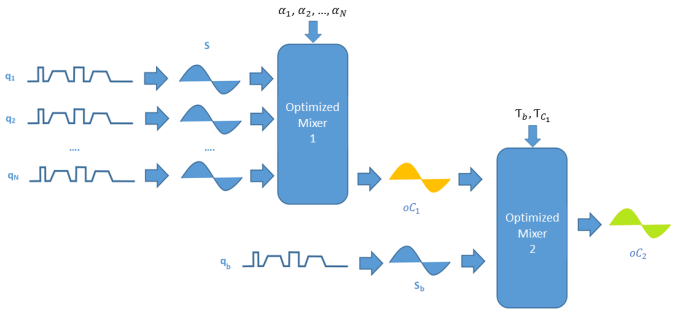

Fig. 2: Overview of enhanced dual-stage correlated diffusion imaging

A detailed description of the steps involved in eD-CDI is presented in sections II-A, II-B, and II-C.

A. Diffusion signal acquisition

Several diffusion signals (S_i) are acquired ($S = \{S_i | i = 1, ..., N\}$), where S_i represents the i^{th} acquired diffusion signal [15]:

$$S_i = S_0 e^{-b_i D} \tag{1}$$

and S_0 is the signal intensity without the diffusion weighting and D represents the strength of the diffusion. The signal loss due to spins diphase is controlled by b_i, which consists of amplitude and duration of the diffusion pulses, gradient intensity and the time between the two pulses and gyromagnetic ratio.

B. Enhanced signal mixing stages

The acquired diffusion signals S are mixed together to produce a signal C_1 that accounts for the local signal attenuation correlation across the N different gradient pulse strengths and timings within a local spatial sub-volume V. The correlated diffusion signal C_1 can be calculated within the diffusion range $[q_1, q_N]$ as follows:

$$C_1(\underline{x}, \alpha_1, ..., \alpha_N) = \int \dots \int S_{q_1}^{\alpha_1}(\underline{x}) \dots S_{q_N}^{\alpha_N}(\underline{x}) \\ f\left(S_{q_1}(\underline{x}), \dots, S_{q_N}(\underline{x}) | V(\underline{x})\right) dS_{q_1}(\underline{x}) \dots dS_{q_N}(\underline{x}) \tag{2}$$

where $\underline{x}$ denotes voxel location and f denotes the conditional joint probability of $S_{q_1}(\underline{x}), \dots, S_{q_N}(\underline{x})$ within the local spatial sub-volume V around $\underline{x}$. For this study, $[q_1, q_N]$ was set at $[0s/mm^2, 2000s/mm^2]$ where diffusion images of $[0s/mm^2, 1000s/mm^2]$ was acquired and high b-value images of $[1300s/mm^2, 2000s/mm^2]$ were computationally constructed using a Bayesian model with the least squares estimation technique [10]. In addition, V was set as a 7 mm^3 spatial sub-volume as it provided a strong cancerous and healthy tissue separation in prostate gland [12]. To compensate for patient movement during the DWI acquisition, diffusion images ($S_q i$) were registered to T2w image with an affine registration algorithm using the patients coordinates.

Once the correlated diffusion signal C_1 was constructed, it is fed to the second signal mixing stage, where C_1 is mixed with an auxiliary diffusion signal (or T2w) S_b to generate the final correlated diffusion signal C_2 as follows:

$$C_2(\underline{x}) = \int \dots \int \exp\left(\tau_b S_b(\underline{x})\right) \cdot \exp\left(\tau_{C_1} C_1(\underline{x})\right) f\left(S_b(\underline{x}), C_1(\underline{x}) | V(\underline{x})\right) dS_b(\underline{x}) dC_1(\underline{x}) \quad (3)$$

where τ_b and τ_{C_1} are the scale factors for S_b and C_1, respectively, and f is the conditional joint probability between S_b and C_1 within the local sub-volume V around $\underline{x}$. For our experiments in this work, we used T2w as S_b signal.

C. Optimization stage

The optimization phase occurs within Mixer 1 and 2 stages where coefficients $\alpha_1 \dots \alpha_N$, τ_b and τ_{C_1} are used to optimize C_1 and C_2 and generate oC_1 and oC_2 to enhance the separability of cancerous and healthy tissues in the final correlated diffusion signal eD-CDI (Equation 4). This is done by maximizing the area under the receiver operating characteristic (ROC) curve (A_z) of oC_2 with respect to a training data in which the tumourous regions have been marked as ground truth. The optimized Mixer 1 and 2 stages then generate an enhanced correlated diffusion signal eD-CDI.

$$[\alpha_1, ..., \alpha_N, \tau_b, \tau_{C_1}] = \arg\max A_z(\underline{x}, \alpha_1, ..., \alpha_N, \tau_b, \tau_{C_1}) \quad (4)$$

III. Experimental Setup

In this section, the details of image acquisition protocols, the imaging data, and the performance measures used in this study are described.

A. Image Data

To evaluate the performance of the proposed enhanced dual-stage correlated diffusion imaging (eD-CDI) method for delineating between cancerous and healthy tissues in prostate gland, the imaging data of 17 patients were used. The images were acquired using a Philips Achieva 3.0T machine at Sunnybrook Health Sciences Centre, Toronto, Ontario, Canada. All data was obtained under the local institutional research ethics board. The age of the patients ranged from 53 to 83. For each patient, the following MRI modalities were obtained: T2w, DWI, and D-CDI. Table I shows the summary of the imaging parameters for the imaging modalities used for the experiments (e.g., displayed field of view (DFOV), resolution, echo time (TE), and repetition time (TR)). For DWI, we used the ADC map for evaluation purposes since it is widely used for DWI in detecting and diagnosing prostate cancer. All imaging modalities were processed in the ProCanVAS (Prostate Cancer Visualization and Analysis System) platform developed at Sunnybrook Research Institute, Toronto, Ontario, Canada, and University of Waterloo, Waterloo, Ontario, Canada.

TABLE I: Summary of imaging parameters

Modality	DFOV (cm^2)	Resolution (mm^3)	TE (ms)	TR (ms)
T2w	22×22	$0.49 \times 0.49 \times 3$	110	4,687
DWI	20×20	$1.56 \times 1.56 \times 3$	61	6,178
D-CDI	20×20	$1.56 \times 1.56 \times 3$	61	6,178
eD-CDI	20×20	$1.56 \times 1.56 \times 3$	61	6,178

B. Evaluation Metrics

To quantitatively evaluate the performance of the proposed eD-CDI modality and in order to compare its performance with other modalities namely T2w, ADC, and D-CDI, the images were studied and marked by an expert radiologist and confirmed by the corresponding histopathology data with Gleason score 6 and above, which was used as the ground truth for our experiments. Each modality was used to generate an ROC curve with respect to the ground-truth data. The optimization for parameters $\alpha_1 \dots \alpha_N$, τ_b and τ_{C_1} in Equation 4 was performed using a leave-one-patient-out cross validation where for each patient data, the set of parameters that maximized the area under the ROC curve for the remaining patients data was used. This experiment was repeated for all four modalities of T2w, ADC, D-CDI, and eD-CDI.

IV. Experimental Results

Table II shows the area under the ROC curve for all four imaging modalities. The ROC curve for each modality is shown in Figure 3.

TABLE II: Evaluation results for prostate cancer detection

Modality	T2w	ADC	D-CDI	eD-CDI
Area under ROC curve	0.55	0.81	0.80	0.86

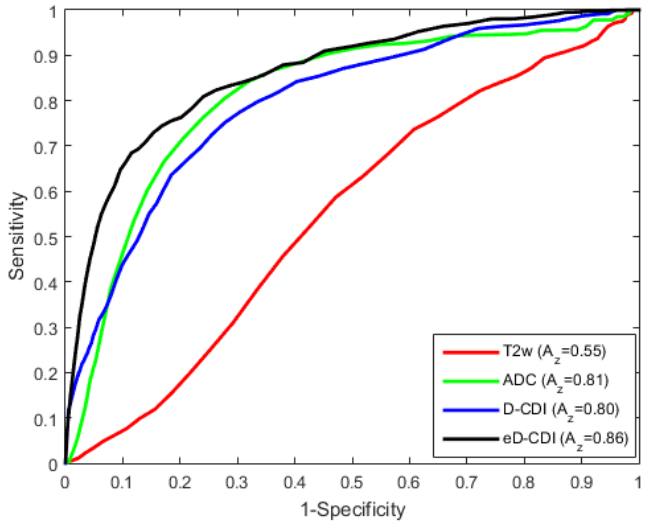

Fig. 3: ROC curves and the area under ROC curves (A_z) for T2w, ADC, D-CDI, and eD-CDI modalities

It is seen that the proposed eD-CDI outperforms the other modalities including the original D-CDI by a large margin

of at least 5% (i.e., 0.86 vs 0.81) in the area under ROC curve. This confirms the promise of eD-CDI for a reliable CAD algorithm for prostate cancer with improved accuracy and consistency of cancer diagnosis.

Figure 4 shows a sample image of T2w, ADC map, D-CDI, and eD-CDI for a confirmed tumourous case. As it can be seen, eD-CDI is able to highlight the cancerous region by clearly darkening the area so it is easier for clinicians to detect the tumour more accurately. Given that mpMRI reading is difficult and usually requires an experienced radiologist to accurately interpret them for diagnosis, the proposed eD-CDI has the potential to harness the information in the mpMRI which cannot be easily deciphered by human experts thus enabling less experienced clinicians to interpret mpMRI more accurately. Moreover, it can play a crucial role in reducing the interobserver variability of interpretations among the clinicians which is an important factor contributing to misdiagnosis of clinically significant prostate cancers.

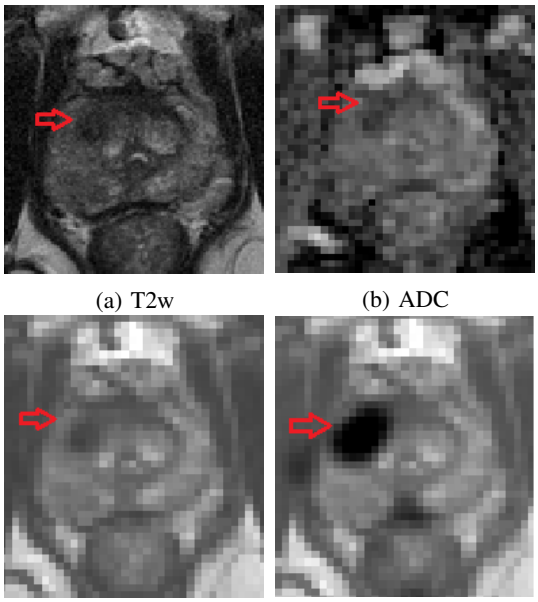

(a) T2w (b) ADC

(c) D-CDI (d) eD-CDI

Fig. 4: A confirmed prostate tumour on different modalities shown by an arrow. The tumor region is dark in eD-CDI, while capturing anatomical structure of the imaged tissue.

V. CONCLUSIONS

In this paper, we introduced enhanced dual-stage correlated diffusion imaging, eD-CDI, which is a new computational diffusion MR imaging modality for prostate cancer detection. The proposed eD-CDI improves the delineation of cancerous and healthy tissues in the prostate gland by utilizing the local correlation among different diffusion signals and by optimizing the way each diffusion signal contributes to the final correlated diffusion signal. The proposed eD-CDI performance was evaluated via a leave-one-patient-out cross-validation and compared against the original unoptimized D-CDI as well as DWI (ADC map) and T2w modalities using 17 patients datasets with confirmed prostate cancer. The results showed that the proposed eD-CDI outperforms the original D-CDI as well as ADC and T2w modalities with a large margin in the area under the ROC curve with respect to the separability of cancerous and healthy tissues within the prostate gland (0.86 vs 0.81). As future work, the proposed eD-CDI will be integrated into a computer-aided detection tool for prostate cancer to investigate the efficacy of eD-CDI in the automatic detection of prostate cancer via a comprehensive texture feature model.

REFERENCES

[1] Canadian Cancer Society, "Canadian Cancer Statistics Special topic : Predictions of the future burden of cancer in Canada," Tech. Rep., 2015.

[2] R. Siegel, D. Naishadham, and A. Jemal, "Cancer Statistics, 2013," *Ca Cancer J CLIN*, vol. 37, no. 2, pp. 408–14, 2013.

[3] G. Andriole, D. Crawford, G. Robert, S. S. Buys, D. Chia, D. Ph, T. R. Church, M. N. Fouad, E. P. Gelmann, P. A. Kvale, D. J. Reding, J. L. Weissfeld, L. A. Yokochi, B. O. Brien, J. D. Clapp, J. M. Rathmell, T. L. Riley, R. B. Hayes, B. S. Kramer, G. Izmirlian, A. B. Miller, P. F. Pinsky, P. C. Prorok, J. K. Gohagan, and C. D. Berg, "Mortality Results from a Randomized Prostate-Cancer Screening Trial," *New England Journal of Medicine*, vol. 360, pp. 1310–1319, 2009.

[4] F. H. Schröder, J. Hugosson, M. J. Roobol, T. L. Tammela, S. Ciatto, V. Nelen, M. Kwiatkowski, M. Lujan, H. Lilja, M. Zappa, L. J. Denis, F. Reck, and A. Auvinen, "Screening and Prostate-Cancer Mortality in a Randomized European Study NEJM," *New England Journal of Medicine*, vol. 360, no. 13, pp. 1320–1328, 2009.

[5] S Loeb, A Vellekoop, HU Ahmed, J Catto, M Emberton, R. Nam, DJ Rosario, V Scattoni, and Y Lotan, "Systematic Review of Complications of prostate biopsy," *Expert review of anticancer therapy*, vol. 13, no. 7, pp. 829–837, 2013.

[6] N. Arumainayagam, H. U. Ahmed, C. M. Moore, A. Freeman, C. Allen, S. A. Sohaib, A. Kirkham, J. van der Meulen, and M. Emberton, "Multiparametric MR imaging for detection of clinically significant prostate cancer: a validation cohort study with transperineal template prostate mapping as the reference standard." *Radiology*, vol. 268, no. 3, pp. 761–9, 2013.

[7] F. Khalvati, A. Wong, and M. A. Haider, "Automated prostate cancer detection via comprehensive multi-parametric magnetic resonance imaging texture feature models." *BMC medical imaging*, vol. 15, no. 1, p. 27, 2015. [Online]. Available: http://www.biomedcentral.com/1471-2342/15/27

[8] A. Cameron, F. Khalvati, M. A. Haider, and A. Wong, "MAPS: A Quantitative Radiomics Approach for Prostate Cancer Detection." *IEEE transactions on bio-medical engineering*, vol. PP, no. 99, p. 1, 2015.

[9] G. Lemaitre, R. Marti, J. Freixenet, J. C. Vilanova, P. M. Walker, and F. Meriaudeau, "Computer-Aided Detection and diagnosis for prostate cancer based on mono and multi-parametric MRI: A review," *Computers in Biology and Medicine*, vol. 60, pp. 8–31, 2015.

[10] J. Glaister, A. Cameron, A. Wong, and M. A. Haider, "Quantitative investigative analysis of tumour separability in the prostate gland using ultra-high b-value computed diffusion imaging," *Proceedings of the Annual International Conference of the IEEE Engineering in Medicine and Biology Society, EMBS*, pp. 420–423, 2012.

[11] M. J. Shafiee, S. A. Haider, A. Wong, D. Lui, A. Cameron, A. Modhafar, P. Fieguth, and M. A. Haider, "Apparent ultra-high b-value diffusion-weighted image reconstruction via hidden conditional random fields," *IEEE Transactions on Medical Imaging*, vol. 34, no. 5, pp. 1111–1124, 2015.

[12] A. Wong, J. Glaister, A. Cameron, and M. Haider, "Correlated diffusion imaging," *BMC medical imaging*, vol. 13, p. 26, 2013.

[13] F. Khalvati, A. Modhafar, A. Cameron, A. Wong, and A. Haider, "A Multi-Parametric Diffusion Magnetic Resonance Imaging Texture Feature Model for Prostate Cancer Analysis," in *International Conference on Medical Image Computing and Computer Assisted Intervention (MICCAI), Computational Di usion MRI*, 2014, pp. 79–88.

[14] A. Wong, F. Khalvati, and M. A. Haider, "Dual-Stage Correlated Diffusion Imaging," in *IEEE International Symposium on Biomedical Imaging*, 2015, pp. 75–78.

[15] P. W. Schaefer, P. E. Grant, and R. G. Gonzalez, "Diffusion-weighted MR Imaging of the Brain," *Radiology*, vol. 217, pp. 331–345, 2000.